Organic LETTERS

Letter

pubs.acs.org/OrgLett

Orthogonally Substituted Benzimidazole-Carbazole Benzene As Universal Hosts for Phosphorescent Organic Light-Emitting Diodes

Jau-Jiun Huang,[†] Yu-Hsiang Hung,[∥] Pei-Ling Ting,[†] Yu-Ning Tsai,[†] Huan-Jie Gao,[∥] Tien-Lung Chiu,*[,∥] Jiun-Haw Lee,[§] Chi-Lin Chen,[†] Pi-Tai Chou,[†] and Man-kit Leung*[,†,‡]

[†]Department of Chemistry, [‡]Institute of Polymer Science and Engineering, [§]Graduate Institute of Photonics and Optoelectronics and Department of Electrical Engineering, National Taiwan University, 1 Roosevelt Road Section 4, Taipei 106, Taiwan, R.O.C.

[∥]Department of Photonics Engineering, Yuan Ze University, 135 Yuan-Tung Road, Taoyuan 32003, Taiwan, R.O.C.

Supporting Information

ABSTRACT: The novel ambipolar hosts of ***o*-CbzBz** and ***o*-DiCbzBz** contain carbazole and benzimidazole through an *ortho*-connection. The orthogonal conformations cause the triplet state to be confined at the carbazole units to secure efficient energy transfer. The phosphorescent organic light-emitting diodes (PhOLEDs) show a high current efficiency, power efficiency, and low efficiency roll-off. ***o*-DiCbzBz** can be used as a host for sky-blue, green, and orange-red PhOLEDs, giving 57.5, 78.4, and 60.3 cd/A, respectively.

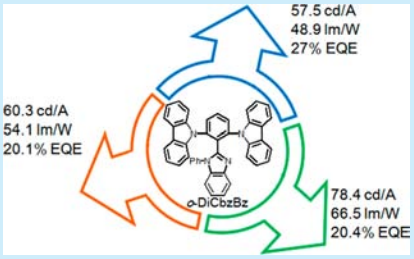

Phosphorescent organic light-emitting diodes (PhOLEDs) have high potential in white light illuminating technology due to their high energy conversion efficiency. However, the nonideal device performance and the short lifetime of blue PhOLEDs, which prohibit them from commercialization, have become the last pieces of the puzzle to be solved.[1] To achieve high PhOLED efficiency, triplet−triplet annihilation (TTA) between phosphorescent emitters has to be avoided.[2] This requires that emitters be isolated by a host matrix that meets several requirements: (i) high triplet energy (E_T) to prevent reverse energy transfer from the emitter to the hosts, (ii) suitable energy level matching for charge injection, (iii) balanced charge transport properties to confine the electron−hole recombination within the emitting layer and to reduce the efficiency roll-off, and (iv) high thermal stability.[3] It would be ideal if the host is universal for blue, green, and red emitters.[4]

Devices from ambipolar hosts usually exhibit good electrical performance.[5] However, intramolecular charge transfer (ICT) leads to a narrower band gap and lower triplet energy. To reduce the ICT effects, disruption of the π-conjugation by introducing nonconjugated linkers such as tetraphenylsilane,[6] a *meta*-connecting benzene ring, or a sterically twisted structure has been studied.[7] Outstanding hosts for a blue PhOLED such as **mNBICz** (54.5 cd/A, 52.2 lm/W, and 26.2%), **mCPCN** (58.7 cd/A, 57.6 lm/W, and 26.4%), **CbBPCb** (53.6 cd/A, 50.6 lm/W, and 30.1%), and *ortho*-(1,2,4-triazole) (carbazole) substituted benzene (52.1 cd/A, 46.1 lm/W, and 24.4%) have been reported.[8]

Benzimidazole is known as an electron-transporting moiety for OLED.[9] Herein we incorporate benzimidazole (Bz)/carbazole (Cbz) in an *ortho*-substituted fashion to give two novel ambipolar hosts denoted as ***o*-CbzBz** and ***o*-DiCbzBz** (Scheme 1; Table 1) that facilitate the hole and electron transport into the emitting layer. Unlike *N,N*-dicarbazolyl-3,5-benzene (*m*CP), steric interactions between the substituents in ***o*-CbzBz** and ***o*-DiCbzBz** keep the substituents perpendicular to the central benzene ring; ICT through π-conjugation is therefore largely reduced so that high T_1 energy could be maintained to fit blue phosphorescent emission. In particular, the sky-blue PhOLEDs device using ***o*-DiCbzBz** for a host gives a maximum current efficiency of 57.5 cd/A, with the EQE up to 27%. ***o*-DiCbzBz** can also be utilized as a universal host for green and orange-red PhOLEDs with maximum efficiency up to 78.4 and 60.3 cd/A, respectively.

Scheme 1. Molecular Structures and the Synthetic Routes of *o*-CbzBz and *o*-DiCbzBz

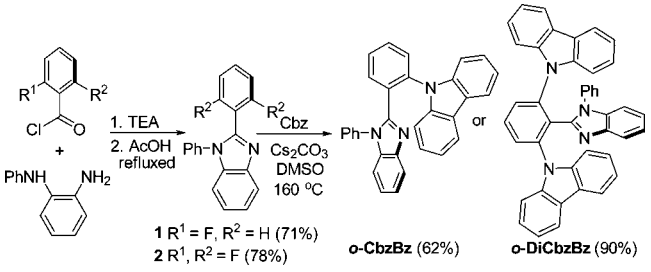

The routes to obtain ***o*-CbzBz** and ***o*-DiCbzBz** are displayed in Scheme 1. The details are reported in the Supporting Information (SI, pp S2−S4). Condensation of 2-fluoro- and 2,6-difluorobenzoyl chloride with 2-PhNH(C_6H_4)NH_2 under acid catalyzed conditions afford **1** and **2**, followed by nucleophilic aromatic substitution with 9*H*-carbazole in

Received: December 22, 2015
Published: February 1, 2016

DOI: 10.1021/acs.orglett.5b03631
Org. Lett. 2016, 18, 672−675

Table 1. Physical Properties of *o*-CbzBz and *o*-DiCbzBz

	$\lambda^{abs}_{(onset)}$ (sol./film, nm)	FL λ_{max} (nm)	E_T (eV)[a]	E_g (sol./film, eV)[b]	HOMO/LUMO (eV)[c]	$T_d/T_g/T_m$ (°C)
o-CbzBz	352/350	396	2.9	3.5/3.5	5.9/2.4	323/77/289
o-DiCbzBz	342/354	418	3.1	3.6/3.5	5.8/2.3	381/117/295

[a]Measured in 2-MeTHF at 77 K; $E_T = 1240.8/\lambda^{Ph}_{(onset)}$. [b]$E_g = 1240.8/\lambda^{abs}_{(onset)}$. [c]Determined through AC-II measurement with thin film (50 nm) and UV absorption spectra; LUMO = HOMO − E_g.

DMSO to give ***o*-CbzBz** and ***o*-DiCbzBz**. Any DMSO residue in the last step was removed by extraction with aqueous NH_4Cl and NaOH.

X-ray crystallography (Figure 1) revealed dihedral angles of 51.02° for C(31)−N(3)−C(19)−C(18) and 52.16° for N(1)−C(13)−C(14)−C(19) for ***o*-CbzBz**. On the other hand, ***o*-DiCbzBz** shows dihedral angles of 86.79° and 81.60° for C(43)−N(4)−C(19)−C(18) and C(20)−N(3)−C(15)−C(14) of the outer Cbz units, indicating that intersubstituent steric interactions are essential to control the conformation of the structures. The dihedral angles of 69.91° for N(1)−C(13)−N(14)−C(19) of the central Bz group is large in comparison to that of ***o*-CbzBz**. The 4.30 Å centroid distance between Bz and Cbz's in ***o*-CbzBz** and 4.37 Å/4.25 Å in ***o*-DiCbzBz**, respectively, are out of the range of strong ground state $\pi-\pi$ interactions.

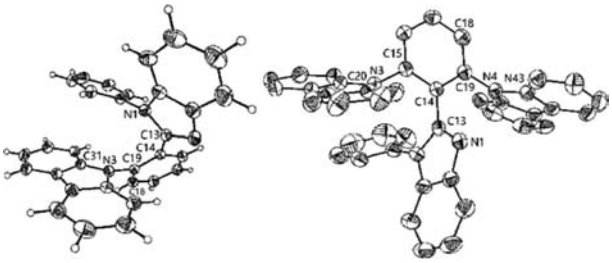

Figure 1. ORTEPs of ***o*-CbzBz** and ***o*-DiCbzBz**.

The thermal stability of ***o*-CbzBz** and ***o*-DiCbzBz** was first illustrated by differential scanning calorimetry (DSC) with a 10 °C/min scanning rate (Figure S5), in which high glass transition temperatures (T_g) at 77 and 117 °C were found, respectively (Table 1). These were far higher than that of *m*CP (60 °C), a common host for PhOLED, and could help to prevent the Ph emitters from phase segregation. A high crystallization temperature (T_c) of 178 °C for ***o*-DiCbzBz** again indicates the stability of the amorphous state under normal device operation conditions. In addition, high decomposition temperatures (T_d: corresponding to 5% weight loss) of 323 and 381 °C were found in the thermogravimetric analysis (TGA); this ensures that the hosts can tolerate the vacuum thermal evaporation conditions in the device fabrication process.

The photophysical properties of ***o*-CbzBz** and ***o*-DiCbzBz** were characterized in tetrahydrofuran (THF) or in 2-methyl tetrahydrofuran (2-MeTHF). The weak absorption at 310−350 nm in THF and the fine vibronic structures are characteristic for the n−π^* transitions of the Cbz units (Figure 2). The absorption bands that peaked at around 300 nm arise from the $\pi-\pi^*$ transitions of the Cbz and Bz chromophores. The spectra are nearly identical with the overlay spectra of *N*-phenylcarbazole (NPC) and Bz, indicating that the ICT in their ground states is weak (Figure S6, measured in THF). The interruption of the π-conjugation by the orthogonal alignment of the aromatic rings is further supported by the DFT calculations, which clearly shows separation of the HOMO and LUMO in ***o*-CbzBz** and ***o*-DiCbzBz**.

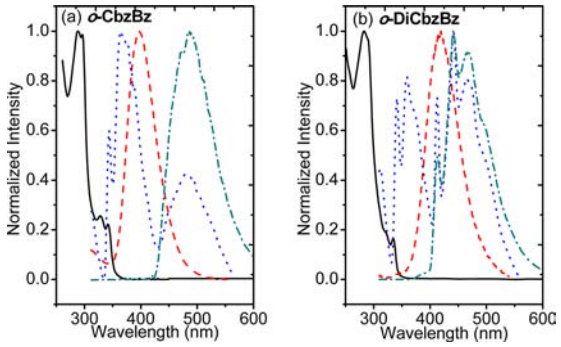

Figure 2. Absorption (—— ——), fluorescence (− − −), low-temperature fluorescence (··· ···), and low-temperature phosphorescence spectra (− · −) of (a) ***o*-CbzBz** and (b) ***o*-DiCbzBz** at 77 K. The excitation wavelength is 290 nm.

At 77 K, both compounds show structured fluorescence (FL) spectra at 350−400 nm in a 2-MeTHF frozen grassy matrix. On the other hand, at room temperature (26 °C) in THF, the structureless FL spectrum peaking at 396 nm for ***o*-CbzBz** and 418 nm for ***o*-DiCbzBz** was respectively observed. The emission maxima show solvatochromism from cyclohexane to MeOH and are shifted up to 50 nm for ***o*-CbzBz** and 35 nm for ***o*-DiCbzBz** (Figure S7). These results indicate that there are at least some degrees of ICT in their excited state. Since the conformation of the donor−acceptor substituents are restricted and the π-conjugation effects should be small in ***o*-CbzBz** and ***o*-DiCbzBz**, the solvato red shifts may arise from the solvent relaxation effects. The actual origins of the ICT characters are pending. However, our X-ray crystallography analysis disclosed that the distance between donor and acceptor is ca. 4.3 Å which may allow charge transfer through space in their S_1 excited states.

The low-temperature phosphorescence (Ph) spectra are quite unexpected. While the observed Ph vibronic pattern of ***o*-DiCbzBz** is similar to that of *m*CP, the structureless pattern of ***o*-CbzBz** is similar to that of *N*-phenylbenzimidazole (BImP).[9b] We attribute this to the coplanar conformation of the Bz unit in ***o*-CbzBz** in the triplet state T_1. As shown in Figure 3, the Bz unit is sterically allowed to stay coplanar with the central benzene unit, leading to an extension of the π-conjugation with

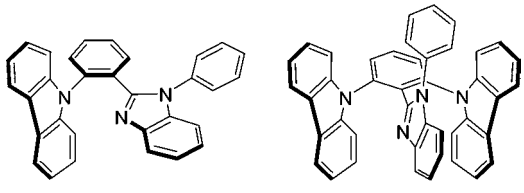

Figure 3. Possible conformation of ***o*-CbzBz** and ***o*-DibzBz** in their T_1 states.

DOI: 10.1021/acs.orglett.5b03631
Org. Lett. 2016, 18, 672−675

a lower E_T of 2.9 eV being recorded. The Ph spectrum of ***o*-CbzBz** therefore shows the characteristic of the Bz unit. On the other hand, in ***o*-DiCbzBz**, the 1,2,3-*ortho*-substituent array prohibits the Bz unit from being coplanar with the central benzene ring. In this situation, the π-conjugation of the Bz unit becomes interrupted, and hence the T_1 state falls onto the Cbz units, with a higher E_T of 3.0 eV being recorded. Nevertheless, the E_T values of both compounds are high enough to prevent reverse energy transfer from FIrpic. Accordingly they can be used as hosts in this study.

***o*-CbzBz** and ***o*-DiCbzBz** are electrochemically active and showed oxidation and reduction waves in their cyclic voltammetry (CV) and differential-pulse voltammetry (DPV) (Figure S8). This observation is in good agreement with our prediction of the ambipolar properties. In the oxidation scan in MeCN, ***o*-CbzBz** and ***o*-DiCbzBz** show an irreversible oxidation wave with E_{DPV} of 0.83−0.84 V with respect to the ferrocene/ferrocenium (Fc/Fc^+) couple. The oxidation potential is very close to that of NPC, indicating that the oxidation should occur on the carbazole units. On the other hand, reduction took place at around −2.60 to −2.70 V in DMF, which is close to that of BImP (−2.55 V), suggesting that the Bz group functions as an electron-accepting unit. In reference to the redox couple of Fc/Fc^+, the HOMO/LUMO levels of 5.8/2.2 eV for ***o*-CbzBz** and 5.8/2.3 eV for ***o*-DiCbzBz** were estimated from the DPV data, using the Forrest approach.[10] The HOMO in the solid thin film was further confirmed by AC-II and the LUMO was estimated according to the equation of LUMO = HOMO − E_g, where E_g is the optical band gap determined from the onset of the lowest absorption band (Figure S9). The HOMO/LUMO of 5.9/2.4 eV for ***o*-CbzBz** and 5.8/2.3 eV for ***o*-DiCbzBz** solid film are close to those of common hole and electron transport layers. This will help to reduce the charge injection energy barrier.

To show the potential of materials as hosts for PhOLED, a series of devices were fabricated with configuration of ITO glass/TAPC (50 nm)/*m*CP (10 nm)/hosts: X% dopant (30 nm)/DPPS (35 nm for ***o*-CbzBz** and 45 nm for ***o*-DiCbzBz** after optimization)/LiF (0.9 nm)/Al (120 nm). The molecular structures of TAPC, DPPS, TAZ, and the dopants including FIrpic, $Ir(PPy)_3$, and $(Bt)_2Ir(acac)$ and their energy level alignment are shown in Figure S11. TAPC and DPPS were used respectively as the hole- and electron-transport layer. Although the actual role of *m*CP is pending, *m*CP may probably act as an exciton block.[11] Without being helped by the *m*CP layer, the device efficiency will significantly drop.

FIrpic, a sky-blue emitter, with the doping level of 12% in ***o*-CbzBz** (device A) and 6% in ***o*-DiCbzBz** (device B), was adopted. The current density−voltage−luminance (*J*−*V*−*L*) characteristics, efficiency performances, and spectra are shown in Figure 4, Figures S12−S17 and summarized in Table 2. The devices, in general, exhibited low turn-on voltage at 3.5−4.0 V (defined as the voltage at 10 cd/m^2). Maximum luminescence (L_{max}) of 14 850 and 11 160 cd/m^2 were achieved at 11.0 and 10.5 V for devices A and B, respectively. However, the performance of device A was inferior to that of device B in many dimensions. For example, although device A showed reasonably good performance with the maximum current efficiency (CE_{max}) of 49.5 cd/A, maximum power efficiency (PE_{max}) of 43.6, and maximum external quantum efficiency (EQE_{max}) of 22.2%, device B achieved even better CE_{max}, PE_{max}, and EQE_{max} (57.5 cd/A, 48.9 lm/W, and 27.0%). Amazingly, the performance of device B at 1000 cd/m^2 remained high, with

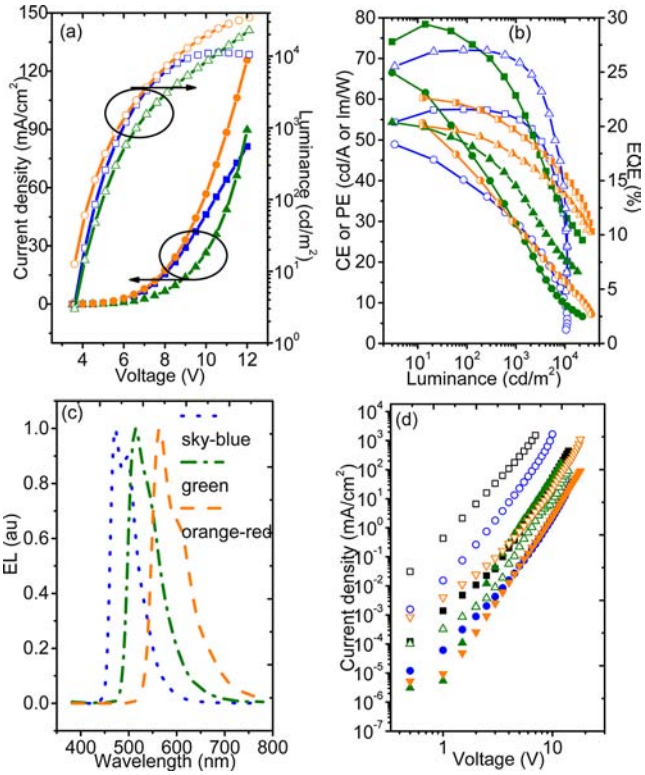

Figure 4. Performances of PhOLEDs with ***o*-DiCbzBz** as the universal host. (a) The *J*−*L*−*V* curves. (b) The CE (square), PE (cycle), and EQE (triangle) of the PhOLEDs: FIrpic-doped (blue and empty); $Ir(ppy)_3$-doped (green and filled); $(Bt)_2Ir(acac)$-doped (orange-red and half-filled). (c) The EL spectra. (d) The plots of current density versus applied electrical voltage for the hole-only (empty) and electron-only (filled) devices: intrinsic (square); FIrpic-doped (cycle), $Ir(ppy)_3$-doped (triangle), and $(Bt)_2Ir(acac)$-doped (inverted-triangle).

the CE of 55.4 cd/A and EQE of 26.0%. Since ***o*-DiCbzBz** showed better performance in the sky-blue PhOLED, it was selected for further research in a high efficiency universal host. In these devices, $Ir(ppy)_3$ (6%) as the green emitter and $(Bt)_2Ir(acac)$ (0.5%) as the orange-red emitter (device D) were respectively doped in ***o*-DiCbzBz** matrix. The $Ir(ppy)_3$-doped device C exhibited L_{max} = 22790 cd/m^2, CE_{max} = 78.4 cd/A, PE_{max} = 66.5 lm/W, and EQE_{max} = 20.4% (Figure 4). The $(Bt)_2Ir(acac)$-doped device D exhibited L_{max} = 34 600 cd/m^2, CE_{max} = 60.3 cd/A, PE_{max} = 54.1 lm/W, and EQE_{max} = 20.1%. The EL spectra for devices B, C, and D are shown in Figure 4c.

To understand the charge-carrier transporting properties of ***o*-DiCbzBz** and the emitter doped (6%) ***o*-DiCbzBz**, the electron-only device (EOD) and hole-only device (HOD) were studied. Figure 4d shows the plots of current density arising from single-charge carriers versus applied electrical voltage of nondoped ***o*-DiCbzBz** and doped ***o*-DiCbzBz**. The hole and electron mobility of ***o*-DiCbzBz** was estimated by trap-free Mott−Gurney law and the trap-relative Poole−Frenkel mode. The hole mobility ($\mu_0 = 3 \times 10^{-6}$ cm^2/(V s)) is about 50 times higher than the electron mobility ($\mu_0 = 6 \times 10^{-8}$ cm^2/(V s)), indicating the intrinsic bipolar property of ***o*-DiCbzBz**.

When doped with FIrpic, the hole and electron mobilities drop by a similar order of magnitude, which is unexpected. FIrpic is a deep electron-trapping center in common host matrix due to the large difference in their LUMO levels. Since the LUMO level difference of 0.6 eV was found between ***o*-**

DOI: 10.1021/acs.orglett.5b03631
Org. Lett. 2016, 18, 672−675

Table 2. EL Characteristics of Various PhOLEDs Devices

device	host	V_{on}[a](V)	L_{max} (cd/m^2)	CE[b](cd/A)	PE[b](lm/W)	EQE[b](%)
A: 12% FIrpic[c]	***o*-CbzBz**	3.5	14 850@11 V	49.5, 47.3	43.6, 26.4	22.2, 21.3
B: 6% FIrpic[c]	***o*-DiCbzBz**	3.7	11 160@10.5 V	57.5, 55.4	48.9, 30.0	27.0, 26.0
C: 6% $Ir(ppy)_3$[d]	***o*-DiCbzBz**	3.8	22 790@12 V	78.4, 60.6	66.5, 29.4	20.4, 14.3
D: 0.5% $(Bt)_2Ir(acac)$[c]	***o*-DiCbzBz**	3.7	34 600@12 V	60.3, 52.0	54.1, 29.1	20.1, 17.3

[a]Turn-on voltage at 10 cd/m^2. [b]The maximum value and the values at 1000 cd/m^2. [c]ITO glass/TAPC (50 nm)/*m*CP (10 nm)/hosts: X% dopant (30 nm)/DPPS (35 nm for ***o*-CbzBz** and 45 nm for ***o*-DiCbzBz**)/LiF (0.9 nm)/Al (120 nm). [d]50 nm for DPPS.

DiCbzBz (2.3 eV) and FIrpic (2.9 eV), the electron-trapping mechanism is expected. In contrast, FIrpic should act as a shallow hole trap because of a small difference in HOMO levels between FIrpic (5.8 eV) and ***o*-DiCbzBz** (5.8 eV).[12] The observation of the hole-mobility drop in the FIrpic doped ***o*-DiCbzBz** is quite unexpected. Nevertheless, the relatively high hole mobility in comparison to the electron mobility secures the position of the recombination zone nearby the cathode. This is important for the high EL efficiency because the exciton quenching phenomenon is usually significant at the *m*CP interface.

In the $(Bt)_2Ir(acac)$ doped ***o*-DiCbzBz**, due to the higher HOMO of $(Bt)_2Ir(acac)$, the hole current drops significantly in comparison to that of the FIrpic doped device. Nevertheless, the apparent hole mobility is still higher than the electron mobility to secure the recombination zone nearby the cathode.

On the other hand, for the $Ir(ppy)_3$ doped devices, although the hole current is higher than the electron current in the low voltage region, the curves cross over at 2 V and the electron current in the EOD becomes slightly higher than that of the HOD at the high voltage region, indicating that the recombination zone may migrate toward the anode under high electrical voltage conditions. This reflects on the relatively large roll-off of the device efficiency.

In conclusion, we demonstrate the use of the *ortho*-substituent steric effect to control orthogonal alignments that successfully interrupt the π-conjugation. High triplet state energy can therefore be maintained that would be beneficial as universal hosts for highly efficient PhOLEDs.

■ ASSOCIATED CONTENT

Supporting Information

The Supporting Information is available free of charge on the ACS Publications website at DOI: 10.1021/acs.orglett.5b03631.

Synthetic procedures, spectral data, AC-II measurements, energy diagram, device performance (PDF)
X-ray data for ***o*-CbzBz** (CIF)
X-ray data for ***o*-DiCbzBz** (CIF)

■ AUTHOR INFORMATION

Corresponding Authors

*E-mail: tlchiu@saturn.yzu.edu.tw (T.-L.C.)
*E-mail: mkleung@ntu.edu.tw (M.-k.L)

Notes

The authors declare no competing financial interest.

■ ACKNOWLEDGMENTS

Ministry of Science and Technology, R.O.C. (MOST 104-2119-M-002-023, 101-2113-M-002-010-MY3, 103-3113-E-155-001, 104-3113-E-155-001, 105-3113-E-155-001, 103-2221-E-155-028-MY3, 104-2221-E-002-156-MY3, and NSC 102-2221-E-002-182-MY3). Prof. Yu-Tai Tao, Institute of Chemistry, Academia Sinica, for discussions and AC-II measurements.

■ REFERENCES

(1) (a) Baldo, M. A.; O'Brien, D. F.; You, Y.; Shoustikov, A.; Sibley, S.; Thompson, M. E.; Forrest, S. R. *Nature* **1998**, *395*, 151−154. (b) Baldo, M. A.; Thompson, M. E.; Forrest, S. R. *Nature* **2000**, *403*, 750−753.

(2) (a) Holmes, R. J.; Forrest, S. R.; Tung, Y.-J.; Kwong, R. C.; Brown, J. J.; Garon, S.; Thompson, M. E. *Appl. Phys. Lett.* **2003**, *82*, 2422−2424. (b) Zhou, G.-J.; Wong, W.-Y.; Yao, B.; Xie, Z.; Wang, L. *J. Mater. Chem.* **2008**, *18*, 1799−1809.

(3) Sun, D.; Ren, Z.; Bryce, M. R.; Yan, S. *J. Mater. Chem. C* **2015**, *3*, 9496−9508.

(4) (a) Lai, C.-C.; Huang, M.-J.; Chou, H.-H.; Liao, C.-Y.; Rajamalli, P.; Cheng, C.-H. *Adv. Funct. Mater.* **2015**, *25*, 5548−5556. (b) Ho, C.-L.; Chi, L.-C.; Hung, W.-Y.; Chen, W.-J.; Lin, Y.-C.; Wu, H.; Mondal, E.; Zhou, G.-J.; Wong, K.-T.; Wong, W.-Y. *J. Mater. Chem.* **2012**, *22*, 215−224. (c) Yang, X.; Zhou, G.; Wong, W.-Y. *Chem. Soc. Rev.* **2015**, *44*, 8484−8575.

(5) (a) Wagner, D.; Hoffmann, S. T.; Heinemeyer, U.; Münster, I.; Köhler, A.; Strohriegl, P. *Chem. Mater.* **2013**, *25*, 3758−3765. (b) Chaskar, A.; Chen, H.-F.; Wong, K.-T. *Adv. Mater.* **2011**, *23*, 3876−3895. (c) Choi, W.-H.; Tan, G.; Sit, W.-Y.; Ho, C.-L.; Chan, C. Y.-H.; Xu, W.; Wong, W.-Y.; So, S.-K. *Org. Electron.* **2015**, *24*, 7−11.

(6) (a) Leung, M.-k.; Yang, W.-H.; Chuang, C.-N.; Lee, J.-H.; Lin, C.-F.; Wei, M.-K.; Liu, Y.-H. *Org. Lett.* **2012**, *14*, 4986−4989. (b) Liu, D.; Du, M.; Chen, D.; Ye, K.; Zhang, Z.; Liu, Y.; Wang, Y. *J. Mater. Chem. C* **2015**, *3*, 4394−4401.

(7) Ding, L.; Dong, S.-C.; Jiang, Z.-Q.; Chen, H.; Liao, L.-S. *Adv. Funct. Mater.* **2015**, *25*, 645−650.

(8) (a) Pan, B.; Wang, B.; Wang, Y.; Xu, P.; Wang, L.; Chen, J.; Ma, D. *J. Mater. Chem. C* **2014**, *2*, 2466−2469. (b) Lin, M.-S.; Yang, S.-J.; Chang, H.-W.; Huang, Y.-H.; Tsai, Y.-T.; Wu, C.-C.; Chou, S.-H.; Mondal, E.; Wong, K.-T. *J. Mater. Chem.* **2012**, *22*, 16114−16120. (c) Lee, C. W.; Lee, J. Y. *Adv. Mater.* **2013**, *25*, 5450−5454. (d) Leung, M.-k.; Hsieh, Y.-H.; Kuo, T.-Y.; Chou, P.-T.; Lee, J.-H.; Chiu, T.-L.; Chen, H.-J. *Org. Lett.* **2013**, *15*, 4694−4697.

(9) (a) Qin, W.; Yang, Z.; Jiang, Y.; Lam, J. W. Y.; Liang, G.; Kwok, H. S.; Tang, B. Z. *Chem. Mater.* **2015**, *27*, 3892−3901. (b) Huang, J.-J.; Leung, M.-k.; Chiu, T.-L.; Chuang, Y.-T.; Chou, P.-T.; Hung, Y.-H. *Org. Lett.* **2014**, *16*, 5398−5401. (c) Liu, M.; Li, X.-L.; Chen, D. C.; Xie, Z.; Cai, X.; Xie, G.; Liu, K.; Tang, J.; Su, S.-J.; Cao, Y. *Adv. Funct. Mater.* **2015**, *25*, 5190−5198.

(10) (a) D'Andrade, B. W.; Datta, S.; Forrest, S. R.; Djurovich, P.; Polikarpov, E.; Thompson, M. E. *Org. Electron.* **2005**, *6*, 11−20. (b) Djurovich, P. I.; Mayo, E. I.; Forrest, S. R.; Thompson, M. E. *Org. Electron.* **2009**, *10*, 515−520.

(11) Mamada, M.; Ergun, S.; Pérez-Bolívar, C.; Anzenbacher, P. *Appl. Phys. Lett.* **2011**, *98*, 073305.

(12) (a) Li, C.; Duan, L.; Li, H.; Qiu, Y. *J. Phys. Chem. C* **2014**, *118*, 10651−10660. (b) Matsusue, N.; Ikame, S.; Suzuki, Y.; Naito, H. *J. Appl. Phys.* **2005**, *97*, 123512.

DOI: 10.1021/acs.orglett.5b03631
Org. Lett. 2016, 18, 672−675